PROTEINS
STRUCTURE ■ FUNCTION ■ BIOINFORMATICS

A QM/MM study of proton transport pathways in a [NiFe] hydrogenase

Ignacio Fdez. Galván,[1]* Anne Volbeda,[2] Juan C. Fontecilla-Camps,[2] and Martin J. Field[1]

[1] Laboratoire de Dynamique Moléculaire, IBS (Institut de Biologie Structurale — Jean-Pierre Ebel), CEA, CNRS, Université Joseph Fourier, F-38027 Grenoble, France

[2] Laboratoire de Cristallographie et Cristallogenèse des Protéines, IBS (Institut de Biologie Structurale — Jean-Pierre Ebel), CEA, CNRS, Université Joseph Fourier, F-38027 Grenoble, France

ABSTRACT

A theoretical QM/MM study of the [NiFe] hydrogenase from* Desulfovibrio fructosovorans *has been performed to investigate possible routes of proton transfer between the active site and the protein surface. We obtained the minimum energy paths, with a modified version of the nudged elastic band method, for a set of proposed pathways. The calculations were carried out for the crystallographic structure and for several structures of the protein obtained from a molecular dynamics simulation. The results show one of the studied pathways to be preferred for transport from the active site to the surface, but the preference is not so strong when transport occurs in the opposite direction.

Proteins 2008; 73:195–203.

Key words: **Desulfovibrio fructosovorans;** ***minimum energy path; nudged elastic band method; molecular dynamics; proton transfer.***

INTRODUCTION

Hydrogenases are enzymes capable of catalyzing both the oxidation of H_2 to $2H^+$ and the reverse reaction, the formation of H_2 from two protons and two electrons. They play a vital role in many anaerobic metabolisms and can be found in bacteria and archaea, as well as in some eukaryotes.[1] The H_2 production function of hydrogenases has generated great interest, as hydrogen has a great potential as a clean energy carrier, provided that it is produced from a clean source like water. This might be achieved through the coupling of hydrogenase with photosystem II, which would allow the electrons and protons liberated from water during photosynthesis to be directly converted into H_2. A major complication is the inactivation of most hydrogenases by O_2, the other product of water photolysis. Much research effort is going on to produce hydrogen from water in a cheap, safe, and convenient way.

A classification of hydrogenases can be established according to the metal composition of their active sites. In [FeFe] hydrogenases, this contains two Fe atoms, whereas in [NiFe] hydrogenases it contains one Ni and one Fe atom.[2] In both types of enzymes, the iron atoms have CO and CN^- as ligands. The metal pairs are bridged and kept in place by thiolate groups. Another common feature is that the active site is deeply buried and connected to the protein surface by a series of Fe—S clusters, which provide a likely pathway for the electrons to be transferred toward or from the redox partners of the enzymes. In addition, hydrophobic tunnels that allow the diffusion of hydrogen molecules to and from the active site have been identified in both types of hydrogenase.[3–6]

The mechanism of the actual reaction catalyzed by these enzymes ($H_2 \rightleftharpoons 2H^+ + 2e^-$) and the different redox states displayed by their active site have been widely studied both theoretically and experimentally.[7–14] Nevertheless, there is still not a clear agreement on the structure–function relationships of the active sites of hydrogenases.

The evidence regarding the proton transfer pathways is relatively scarce. It is in general assumed that the mechanism for proton transport inside the protein is related to the Grotthuss mechanism, in which the location of an excess proton is displaced by a series of individual proton transfers between water molecules and amino acid residues with acid–base properties.[15,16] There have been several possible routes proposed for proton transfer to and from the active site of hydrogenases.[17–19] A wide agreement exists for the involvement, after H_2 cleavage, of a terminal cysteine ligand of the nickel atom.[2] Moreover, recent experimental evidence has shown that a neighboring glutamate residue is essential for the H^+/D^+ exchange function,[20] leading to the conclusion that

Grant sponsor: Secretaría de Estado de Universidades e Investigación, Spanish Ministerio de Educación y Ciencia.
*Correspondence to: Ignacio Fdez. Galván, Química Física, Universidad de Extremadura, Avda. de Elvas s/n, 06071 Badajoz, Spain. E-mail: jellby@unex.es
Received 18 December 2007; Accepted 12 February 2008
Published online 15 April 2008 in Wiley InterScience (www.interscience.wiley.com). DOI: 10.1002/prot.22045

proton transfer to this residue is the next step in the process. From here the distance to the protein surface is still rather large, and the pathways of escape remain to be determined. It is of great interest to increase our understanding of proton transfer in hydrogenase, as this is crucial for enzymatic hydrogen production.

In this work, we study theoretically the proton transport in a [NiFe] hydrogenase from *Desulfovibrio fructosovorans* and attempt to identify pathways for the proton transport between the active site and the protein surface. We used a combined quantum mechanics and molecular mechanics (QM/MM) potential and a modified nudged elastic band (NEB) algorithm to optimize energy profiles for possible paths. The minimum energy paths (MEPs) thus obtained allow us to compare the energy barriers of the different pathways.

While this manuscript was in preparation, an article of Teixeira *et al.* appeared,[21] which also addresses the issue of proton transport pathways in a [NiFe]-hydrogenase. They worked on the enzyme from *D. gigas* and employed different, but complementary, techniques to the ones that we use here. We will compare their results with ours in more detail in the final section.

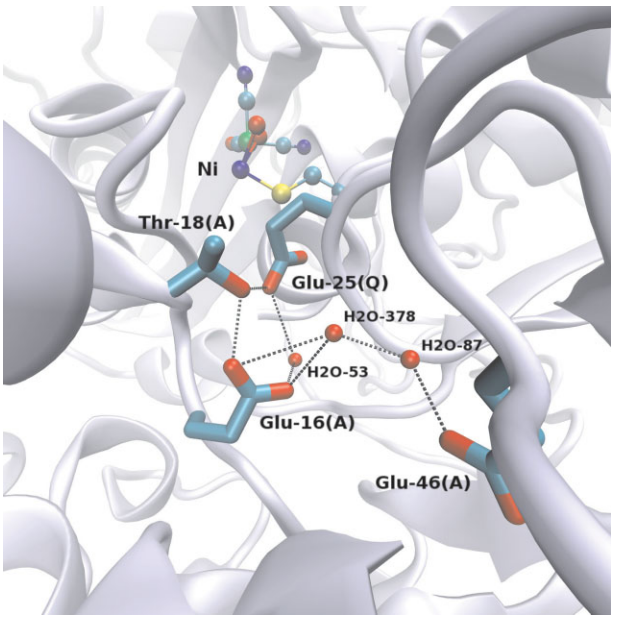

Figure 1

First hypothesized proton transport pathway in hydrogenase, Glu-25(Q) → Glu-46(A). Image created with VMD.[23]

METHOD

We have tackled the problem of finding the pathways for proton transport in a hydrogenase by performing atomistic QM/MM calculations on a complete model of the system. Given a particular pathway, we obtain the MEP for the process, which is the energetically optimum path in configuration space between reactant and product structures. If determined properly, the energy maxima in a MEP approximate the saddle points (transition states) for the reaction while minima represent more or less stable intermediate states. By comparing the MEPs obtained for different pathways in the model, we hope to establish the preference or likelihood of the corresponding pathways in the real system.

There has been much speculation about the routes of proton transfer in [NiFe] hydrogenases.[19,22] Based on extensive geometrical analyses of networks of protonatable groups in the crystallographic structures, using both visual inspection and calculation, two basic pathways appear possible. In the hydrogenase from *D. fructosovorans* (PDB code: 1YQW, subunits A and Q), which is the structure that we use in our calculations, both pathways start at GLU-25(Q), as this residue is the initial acceptor for departing protons produced in the [NiFe] active site.[20] The first pathway (Fig. 1) goes through Glu-16(A) to Glu-46(A), which is at the bottom of a groove on the protein surface. This pathway entails five proton-transfer steps and, in the crystal structure of the protein, has a length of around 14–15 Å. The second pathway (Fig. 2) goes through the C-terminal His-549(Q) to Glu-53(Q) and then onto waters, lying close to the surface, that surround a nearby Mg^{2+} cation.[19,22] This second pathway is around 27 Å long and entails not less than 10 proton-transfer steps. Based on the length of these pathways, the first would seem more attractive.

Although there are only two basic pathways, many more were in fact studied. First, each basic path had at least two variants, depending on the exact route followed by the protons. Second, paths were calculated for structures of the protein derived from molecular dynamics (MD) simulation, in addition to the experimental crystallographic one. This is essential to see how sensitive the MEP energy profiles for a given pathway are to structural perturbations.

Model building

The enzyme model for the QM/MM calculations was built from the crystal structure of the [NiFe] hydrogenase from *D. fructosovorans*, obtained by X-ray diffraction at a resolution of 1.8 Å, and published with the PDB code 1YQW.[13] The crystallographic model consists of three hydrogenase heterodimers. The unit formed by chains A (small subunit) and Q (large subunit) was isolated, together with the solvent molecules inside and surrounding it (bicarbonate and glycerol molecules were replaced by waters). Residues 1 and 2 from the A chain and 1–5 from the Q chain are absent in the pdb file; since these

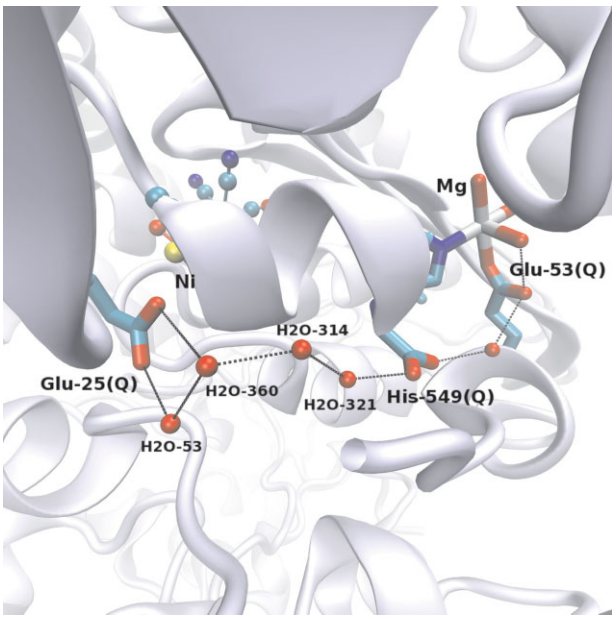

Figure 2

Second hypothesized proton transport pathway in hydrogenase, Glu-25(Q) → Glu-53(Q). Image created with VMD.[23]

portions are at the protein surface and far from the regions concerned in this work, their influence is presumed to be negligible, and thus, residues Ala-3(A) and Pro-6(Q) were converted to N-terminal residues. In the cases where alternate locations are given in the PDB structure, the location with a higher occupancy was chosen.

The aforementioned structure corresponds to an inactive form of the hydrogenase. To build a model for the active form, the active center was modeled after the crystal structure of a reduced hydrogenase of the same organism obtained at 2.1 Å resolution (Volbeda A, unpublished), which is similar to other published structures of the reduced enzyme.[24,25] This reduced structure is almost identical to 1YQW (rms deviation of the backbone atoms: 0.19 Å), the most noticeable differences being around the [NiFe] center. For this reason the coordinates of the atoms in residues NI and FCO, as well as atoms S_γ and C_β from Cys-72(Q), Cys-75(Q), Cys-543(Q), and Cys-546(Q), were copied from the reduced structure. Additionally, the O atom close to S_γ in Cys-75(Q) (assigned to H_2O-557(Q) in 1YQW) was removed in order to transform the sulfenate into a thiolate, and the PER residue, representing a hydroperoxide anion, was substituted with a hydride at the O_1 position, assumed to be present in the active form.[2,26] The partially occupied FE2 residue in 1YQW that is bound to the C-terminal His-549 of the large subunit was replaced by a Mg^{2+} ion.

The position of the hydride with respect to the [NiFe] center was optimized, in vacuo, with DFT quantum chemical calculations (B3LYP functional, 6-31+G(d) basis set) of the system formed by residues NI, FCO, and HYD (hydride). Atomic charges for these atoms were obtained from the resulting wavefunction with the CHELPG method.[27] The charges for the FS3 and FS4 residues were obtained from similar calculations. In all quantum calculations, NI was modeled as Ni^{II} with low spin. The Fe—S clusters were assigned as $[Fe_4S_4]^{2+}$ and $[Fe_3S_4]^{+}$ with low spin as well. Although some X-ray absorption spectroscopy experiments[28] and DFT calculations[29] suggest the presence of high spin Ni^{II}, the spin state was found to have a rather small effect on the atomic charges obtained with CHELPG. The sensitivity of the results to a change in oxidation state of the nickel and Fe—S clusters was also tested, but no significant differences were found (see Results and discussion, later).

The OPLS-AA force field was used as the MM potential.[30] Standard parameters were taken for all atoms and groups except for the metallic centers. For these, only nonbonding parameters were needed, because the geometries of the Fe—S clusters (FS3 and FS4) and the active center residues (NI, FCO, HYD) were kept fixed in all calculations. Charges for the atoms in these groups were obtained from the DFT calculations discussed earlier, whereas the Lennard-Jones parameters were all standard, except for the Ni atom which was given the same parameters as Fe. The Cys residues bonded to Fe and Ni were deprotonated and represented as thiolates.

Hydrogens were added to the structure and their positions were optimized. The pK_as for the different residues were estimated in two different ways using the PROPKA[31] and UHBD[32] programs. From this information and with confirmation by visual inspection, the most likely tautomer was assigned for each His residue: histidines 5, 13, 92, and 184 from chain A and 27, 66, 79, 113, 115, 118, 121, 123, 188, 210, 228, 349, 419, and 481 from chain Q were protonated at the N_ε atom; histidines 204, 305, and 538 from chain Q were protonated at both the N_ε and N_δ atoms; and all other histidines were protonated at the N_δ atom. All other protonable side chains were set to their standard states in aqueous solution at pH 7. Only water molecules present in the crystal structure were included in the model (i.e., no additional solvent was added), since the calculations that were performed involved zones buried quite deep within the protein. The final model consisted of 14,649 atoms.

Computational details

To get different starting structures for the pathway calculations that showed some variability in their hydrogen-bond networks, an MD simulation was run on the system. During this run, the positions of the metallic centers were kept frozen, as mentioned earlier, and the positions

of the other heavy atoms were held in the vicinity of their positions in the crystallographic structure with a weak harmonic force constant of 2.0 kJ mol^{-1} $Å^{-2}$. The time step for the simulation was 1 fs and 26 ps of dynamics was run (1 ps of equilibration followed by 25 ps of data collection) at a temperature of 300 K using a Langevin thermostat with a collision frequency of 25 ps^{-1}. From the resulting trajectory, seven configurations were selected and the reaction paths (see later) were computed for each of them, as well as for the crystal structure. With respect to the starting, crystallographic structure, the rms coordinate deviations of the dynamics structures was between 0.86 and 0.96 Å for the heavy atoms (0.43–0.57 Å for the backbone atoms only).

For each reaction path studied, the following procedure was carried out. The residues affected by the proton transfer (the QM region) were treated with the PDDG/PM3[33] semiempirical QM method, the rest of the system (the MM region) was described with the aforementioned MM force field (OPLS-AA). The number of atoms in the QM region varies between 39 and 52, depending on the path studied. All residues within 12.0 Å from any of the oxygen atoms implied in the proton transfer were allowed to move (except the atoms of the metallic centers) and all atoms further than 12.0 Å were held fixed. The number of moving atoms varies between 1604 and 2274. This is necessary to reduce the number of degrees of freedom in the optimization which would otherwise affect NEB convergence and introduce too much noise into the results. A proton was added to the system and the initial and final states were optimized. When a specific pathway is studied, it defines the location of the initial excess proton and the particular rearrangement of O—H bonds occurring in the final state, which in turn defines the location of the final excess proton.

The MEP between the initial and final states was optimized with an improved version of the NEB method.[34] Briefly, the NEB method works by representing the MEP between two fixed structures as a set of discrete intermediate structures called "images." The best approximation to a MEP is obtained by minimizing the total force perpendicular to the path on each image using an iterative procedure, while keeping the images evenly spaced in configuration space. The improved version employs a parametric spline representation of the path and a second-order optimization method for the minimization of the force on each image.[35] Each path was first calculated with 25 images and then refined with 51 images. Convergence was achieved when the rms force on each image was lower than 1.0 kJ mol^{-1} $Å^{-1}$.

For the MEPs calculated from the crystal structure, a corrected energy profile was calculated using a higher level DFT method. For each image on the path the in vacuo PDDG/PM3 energy of the QM region was subtracted from the total QM/MM energy (E) and, in exchange, the in vacuo B3LYP/6-31G** energy of the QM region was added. This results in a corrected energy E' with a DFT term for the QM part, a semiempirical/MM term for the electrostatic interaction between QM and MM parts, and an MM term for the QM/MM Lennard-Jones interaction and for the pure MM part. This procedure only gives a first-order estimate of what the DFT QM/MM energy profile would look like as it assumes that the intermediate MEP structures obtained with the semiempirical calculations are correct, that the DFT QM/MM electrostatic interaction energies are the same as their semiempirical equivalents and that the only differences arise from those in the intrinsic QM energies.

All QM/MM modeling, simulations, and NEB calculations were performed with the DYNAMO library.[36] QM (DFT) calculations were performed with the Gaussian-98 program.[37]

RESULTS AND DISCUSSION

The two basic pathways introduced earlier were studied using the crystallographic structure and seven structures derived from the MD simulation as starting points. For practical purposes, both pathways were split in two sections, and the four resulting sections were studied independently. The results obtained using the crystal structure as the initial structure will be presented first in detail and those for the dynamical structures afterwards.

First pathway: Glu-25(Q) → Glu-46(A)

In the first pathway (Fig. 1), the initial section is the proton transfer from Glu-25(Q) to Glu-16(A). There are two possibilities: the proton can be transferred through Thr-18(A) and then to $O_{\varepsilon 2}$ of Glu-16(A), or through a water molecule (H_2O-53) and then to $O_{\varepsilon 1}$ of Glu-16(A). The MEPs for both possibilities were obtained and the energy profiles are shown in Fig. 3. In each profile, there are two barriers corresponding to the two proton transfer steps that occur. In this and equivalent figures the profiles shown correspond to an interpolating cubic spline[35,38] of the MEP data.

It must be noted that the "normalized path length" shown in the graphs is not a direct representation of the excess proton location, but rather a kind of general reaction or event coordinate. The ξ coordinate represents the change in the whole system structure as it proceeds from reactants ($\xi = 0$) to products ($\xi = 1$). Because of the way the NEB method works, there is not an obvious definition of ξ, and the correspondence between its value and particular structures (such as the location of the excess proton) can only be established a posteriori, and will be different for every path. In the graphs, the location of the excess proton, when it can be established, is marked for each curve.

Table I lists the main energetic features of this section of the pathway. For both possibilities, the results show

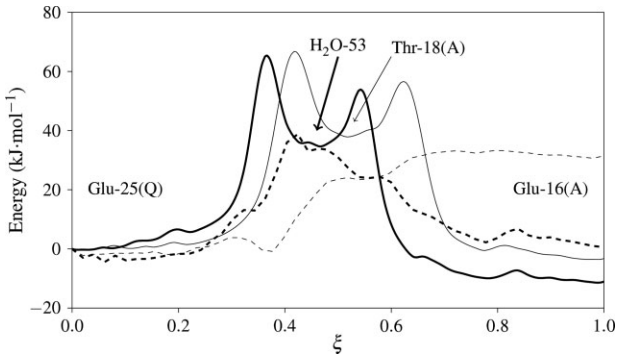

Figure 3

Energy profiles for the proton transport Glu-25(Q) → Glu-16(A). Thick line: the branch through H_2O-53; thin line: the branch through Thr-18(A). The dashed lines are the ab initio corrected energies. ξ is the normalized path length. The labels mark the approximate location of the excess proton.

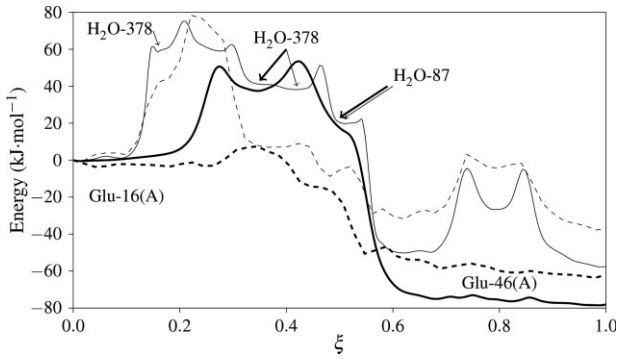

Figure 4

Energy profiles for the proton transport Glu-16(A) → Glu-46(A). Thick line: the branch from $O_{\varepsilon 1}$; thin line: the branch from $O_{\varepsilon 2}$. The dashed lines are the ab initio corrected energies. ξ is the normalized path length. The labels mark the approximate location of the excess proton.

that ΔE is small (-3.3 kJ mol^{-1} or -11.0 kJ mol^{-1}) and the activation energy, which is the highest energy along the calculated MEP, $\Delta^{\ddagger}E$ is around 65 kJ mol^{-1}.

In the second section of the pathway, the proton is transferred from Glu-16(A) to Glu-46(A) through two intermediate water molecules (numbered 378 and 87). As a starting point, the initial excess proton can be bonded to either the $O_{\varepsilon 1}$ or $O_{\varepsilon 2}$ of Glu-16(A), and both possibilities were tested. The energy profiles obtained for this second section appear in Fig. 4. The peaks and shoulders in the profiles correspond to three proton-transfer steps. In the curve corresponding to the transfer from $O_{\varepsilon 2}$, the twin peaks around $\xi = 0.8$ are caused by a water molecule changing its orientation and should not be considered in the proton transport process (it may be called a "parasite event"). Also, in this curve, from $\xi \simeq 0.2$ to $\xi \simeq 0.4$ the excess proton remains localized in H_2O-378, so that the peaks at $\xi = 0.2$ and $\xi = 0.3$ correspond to a water movement and not an actual proton transfer step.

The energy results for the second section of the pathway are also displayed in Table I. The ΔE is now larger in absolute value, -50 kJ mol^{-1} or -80 kJ mol^{-1}, but $\Delta^{\ddagger}E$ has a similar magnitude to the first section, between 55 and 75 kJ mol^{-1}.

Although the energies are not strictly comparable, because different residues are included in the QM region in the different calculations, we can combine information for the two sections and get, for the whole pathway a ΔE of between -55 kJ mol^{-1} and -90 kJ mol^{-1} and a $\Delta^{\ddagger}E$ of around 65–70 kJ mol^{-1} for the two branches (through Thr-18(A) or H_2O-53).

Second pathway: Glu-25(Q) → Glu-53(Q)

For the second pathway (Fig. 2), the initial section involves proton transport from Glu-25(Q) to His-549(Q). There are four water molecules (numbered 53, 360, 314, and 321) joining these two residues. The proton can be transported either through all four water molecules (first transfer to H_2O-53), or just the last three of them (first transfer to H_2O-360). Note that H_2O-53 is also involved in the first pathway. The MEP profiles are shown in Figure 5. Here, the first low peak, at around $\xi = 0.2$ corresponds to the movement of H_2O-360 toward Glu-25(Q) (thin line) and to the proton transfer from Glu-25(Q) to H_2O-53 (thick line), whereas the energy increase up to the plateau at $\xi \simeq 0.5$ represents the

Table I

Energy Difference and "Activation" Energy (in kJ mol^{-1}) for the Proton Transport Glu-25(Q)→Glu-46(A) (First Pathway)

First section (Fig. 3)			Second section (Fig. 4)		
Intermediate	ΔE	$\Delta^{\ddagger}E$		ΔE	$\Delta^{\ddagger}E$
Thr-18(A)	−3.3	66.7	$O_{\varepsilon 2}$	−50.2	75.3
H_2O-53	−11.0	65.3	$O_{\varepsilon 1}$	−78.1	53.5

Table II

Energy Difference and "Activation" Energy (in kJ mol^{-1}) for the Proton Transport Glu-25(Q)→Glu-53(Q) (Second Pathway)

First section (Fig. 5)			Second section (Fig. 6)	
First transfer	ΔE	$\Delta^{\ddagger}E$	ΔE	$\Delta^{\ddagger}E$
H_2O-53	107.5	239.4	39.8	105.9
H_2O-360	74.4	222.1		

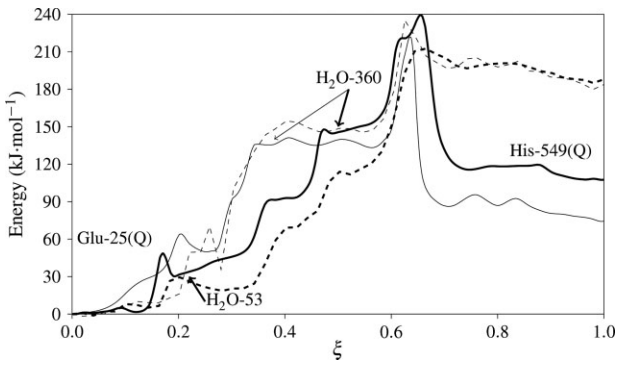

Figure 5

Energy profiles for the proton transport Glu-25(Q) → His-549(Q). Thick line: the branch through H_2O-53; thin line: the branch through H_2O-360. The dashed lines are the ab initio corrected energies. ξ is the normalized path length. The labels mark the approximate location of the excess proton.

movement of water molecules and a proton transfer to H_2O-360. The final high peak at $\xi \simeq 0.6$ corresponds to the last three proton transfer steps which are almost simultaneous ("concerted"). In both MEPs, the final proton transfer from H_2O-321 to His-549(Q) occurs slightly before the protons are transferred to H_2O-314 and H_2O-321, as can be seen in the shoulder at $\xi = 0.6$ of the thick line in Figure 5.

Table II shows the energies for the two possibilities. For both, the ΔE and $\Delta^{\ddagger}E$ values are high, more than 70 and 220 kJ mol^{-1}, respectively, but the option with only three participating water molecules seems to be slightly favored.

The high energy increase when the proton moves along this pathway can be understood from the structure in this region. In the first portion of the pathway, as in the other studied pathway, the environment of the water molecules provides proton donor and acceptor groups that keep the waters in the correct orientation for proton transport (with one hydrogen pointing to another water molecule and the other hydrogen outside the water "chain"). By contrast, the last two water molecules do not have such a benign environment and H_2O-321, in particular, lacks any good proton acceptor group around it, apart from the neighboring residues involved in the proton transport pathway. This lack of hydrogen-bonding reduces the stability of the structures in this region that contain the excess proton.

The second section of this pathway was considered only until the excess proton reaches the Glu-53(Q) carboxyl group. This residue is coordinated to the Mg^{2+} ion, which has three other water ligands and lies close to the protein surface. The proton is first transferred from His-549(Q) to an intermediate water molecule (H_2O-404) and then to Glu-53(Q). Before the first step, the proton has to transfer between the carboxyl oxygens of the C-terminal His-549(Q), or the carboxyl group has to rotate. Both possibilities were tried, but only the first one (intraresidue proton transfer) led to a stable path (Fig. 6). The peak at $\xi = 0.4$ corresponds to this intraresidue proton transfer, while the peak at $\xi = 0.8$ represents the two other transfers that occur simultaneously. The ΔE and $\Delta^{\ddagger}E$ for this section are around 40 and 105 kJ mol^{-1}, respectively, as shown in Table II.

Different oxidation states

In order to test the sensitivity of the results to the partial charges assigned to the [FeS] clusters and [NiFe] center, the MEP calculations above were repeated for systems in which the clusters were modeled as $[Fe_4S_4]^+$ and $[Fe_3S_4]$ or the nickel atom as Ni^{III}. The results were qualitatively and quantitatively very similar to those shown in the previous sections and so will not be presented separately. The implication is that the proton transfer, once it is underway, is not significantly affected by charge density changes that occur at the active site either during catalysis or due to electron transfer. However, this does not mean that the proton transfer function of hydrogenase and these other processes are uncoupled. Thus, George *et al.* found that the Ni—C state can only heterolytically cleave H_2 when the proximal cluster is oxidized, suggesting that the resulting proton can only escape when the active site first loses one electron.[39] Likewise, the redox potentials of the active site and the proximal Fe—S cluster are pH-dependent, suggesting that redox change is coupled to changes in protonation state, although not necessarily to that of the proton-transfer tunnels.

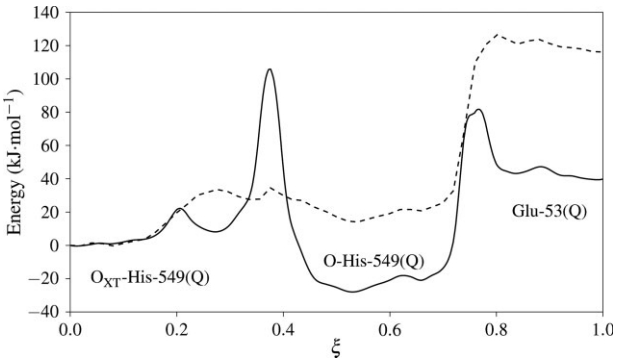

Figure 6

Energy profile for the proton transport His-549(Q) → Glu-53(Q). The dashed line is the ab initio corrected energy. ξ is the normalized path length. The labels mark the approximate location of the excess proton.

Table III
Average and Standard Deviation of the Energy Difference and "Activation" Energy (in kJ mol^{-1}) for the Proton Transport Glu-25(Q)→Glu-46(A)

	First section			Second section	
Intermediate	ΔE	$\Delta^{\ddagger}E$		ΔE	$\Delta^{\ddagger}E$
Thr-18(A)	8.4 ± 18.0	85.5 ± 3.0	$O_{\varepsilon 2}$	−16.9 ± 27.3	92.7 ± 18.3
H_2O-53	−29.6 ± 17.5	60.5 ± 7.2	$O_{\varepsilon 1}$	−19.9 ± 19.3	76.7 ± 6.5

Table V
Ab Initio Corrected Energy Difference and "Activation" Energy (in kJ mol^{-1}) for the Proton Transport Glu-25(Q)→Glu-46(A)

	First section (Fig. 3)			Second section (Fig. 4)	
Intermediate	$\Delta E'$	$\Delta^{\ddagger}E'$		$\Delta E'$	$\Delta^{\ddagger}E'$
Thr-18(A)	31.5	33.3	$O_{\varepsilon 2}$	−37.0	78.4
H_2O-53	0.6	38.8	$O_{\varepsilon 1}$	−62.0	7.5

Results from other initial structures

MEP calculations of the same paths were performed starting with structures obtained from a MD simulation in which the heavy atoms were restrained to their crystal positions, as explained in Method section. The shapes of the energy profiles are, in general, similar to those shown earlier, although with some variation, but the differences are not significant and so they will not be shown here.

The average reaction and activation energies and their standard deviations are displayed in Tables III and IV for the first and second paths, respectively. These values correspond to the seven additional structures obtained from the MDs, and do not include the results from the crystal structure, presented in the previous sections.

The results agree roughly with those from the crystal structure. For the first pathway, an overall $\Delta^{\ddagger}E$ value of around 60 kJ mol^{-1} can be estimated when the first transfer takes place through the H_2O-53 molecule, whereas transfer through Thr-18(A) seems less favored, with an activation energy of some 100 kJ mol^{-1}. In both cases, the process is energetically favored and has a negative ΔE, but more so for the H_2O-53 branch. The second pathway shows higher values than in the crystal structure for both ΔE and $\Delta^{\ddagger}E$. The overall energy barrier is greater than 150 kJ mol^{-1} and reaction energy is now positive and greater than 100 kJ mol^{-1}.

By comparing the global results for the two pathways, the first seems to be more likely as a route for the protons out of the protein. However, the reaction catalyzed by hydrogenase is reversible, and there must also be some way for the protons to get inside the protein from the surrounding medium. In principle, the same proton transport pathways could work in both senses. When the reverse process is considered, the signs of the ΔE change and the $\Delta^{\ddagger}E$ should be calculated with respect to the opposite end of the path. In this case, the activation barrier for both pathways becomes close to 100 kJ mol^{-1}, although the second pathway is favored based on the value of ΔE alone.

Ab initio corrections

Ab initio corrections for the two pathways were estimated for the MEPs obtained from the crystal structure. The results for the first pathway are shown in Table V (cf. Table I). In general, the values of $\Delta E'$ tend to be smaller in absolute value than the corresponding ΔE values and, most important, the $\Delta^{\ddagger}E'$ values are considerably smaller, meaning that the semiempirical QM/MM activation energies are probably overestimated. In Figures 3 and 4 the corrected profiles are represented with dashed lines. Except for one case, the activation barriers decrease significantly or almost disappear.

The results obtained for the second pathway are shown in Table VI (cf. Table II). In the first section, the $\Delta^{\ddagger}E'$ values are not significantly affected, but the $\Delta E'$ are much larger than the semiempirical ΔE values. In the second section, both quantities, $\Delta^{\ddagger}E'$ and $\Delta E'$ become larger, but now $\Delta E'$ is almost as high as $\Delta^{\ddagger}E'$, as also happens in the first section. The corrected profiles are shown as dashed lines in Figures 5 and 6. It is significant that the barrier for the intra-residue proton transfer (the peak at $\xi \simeq 0.4$ in Fig. 6) practically vanishes.

Table IV
Average and Standard Deviation of the Energy Difference and "Activation" Energy (in kJ/mol^{-1}) for the Proton Transport Glu-25(Q)→Glu-53(Q)

	First section		Second section	
First transfer	ΔE	$\Delta^{\ddagger}E$	ΔE	$\Delta^{\ddagger}E$
H_2O-53	113.2 ± 34.8	218.6 ± 50.0	55.7 ± 7.7	115.3 ± 14.8
H_2O-360	60.5 ± 30.8	167.7 ± 41.4		

Table VI
Ab Initio Corrected Energy Difference and "Activation" Energy (in kJ mol^{-1}) for the Proton Transport Glu-25(Q)→Glu-53(Q)

	First section (Fig. 5)		Second section (Fig. 6)	
First transfer	$\Delta E'$	$\Delta^{\ddagger}E'$	$\Delta E'$	$\Delta^{\ddagger}E'$
H_2O-53	183.8	235.3	116.1	126.5
H_2O-360	187.9	212.5		

By extrapolating these correction results to the paths obtained from other structures, we can estimate that the activation energies for the first pathways would be reduced by around 50%, while the values for the second pathway would remain high (more than 100 kJ mol^{-1}) and the ΔE would also become higher. This would result in a stronger preference for the first pathway when considering the proton transport out of the protein, with a calculated activation barrier of 40 kJ mol^{-1}. But if the reverse process is considered, the activation energies for the second pathway seem to be greatly reduced and ΔE would be even more favorable. The results would then suggest a preference for the second pathway when the proton transport occurs from outside the protein to the active site.

In their recent work, Teixeira *et al.*[21] propose a pathway for both directions of transport that practically overlaps with the first pathway that we have studied here. They also considered the pathway corresponding to our second one (through the waters coordinating the Mg_2^+ ion), but find that the first is preferred. An interesting point is whether the water molecules coordinated to the Mg_2^+ are suitable for transporting protons. Although waters in $[Mg(H_2O)_6^{2+}]$ could easily participate in proton transport, the complex environment of the magnesium in hydrogenase could make it harder for the remaining waters.[40] This would further disfavor the second pathway, and thus make the first pathway more likely for the proton transport in both directions, as Teixeira *et al.* suggest.

A comparison of protonation states shows that His-13(A) and His-27(Q) were singly protonated in our simulations but doubly protonated in the *D. gigas* protein studied by Teixeira et al. It is possible that these residues could play a role in proton transfer since they are in the vicinity of the first pathway. His-27(Q) is located closest as it lies between Glu-16(A) and Glu-46(A), and it could also transport a proton through a ring rotation. These possibilities would add another branch to the second portion of the first pathway but have not been investigated in the present work, because the other competing branches appeared to be the more feasible. In any case, proton transfer with a lower energy barrier via this extra branch would only reinforce the preference of the first pathway over the second.

CONCLUSIONS

Two main proton-transport pathways in the [NiFe] hydrogenase from *Desulfovibrio fructosovorans* have been studied with a semiempirical QM/MM method and their MEPs have been obtained. The MEPs have been calculated for the crystal structure and a number of structures obtained from a constrained MD simulation. Higher level quantum chemical (DFT) corrections were also made to some of the calculated energy profiles.

As a general conclusion, it appears that the pathway, involving proton transfer via Glu-25(Q), Glu-16(A), and Glu-46(A), seems to be most likely, with an estimated activation barrier of around 40–60 kJ mol^{-1}. For the second pathway, which involves Glu-25(Q), His-549(Q), and Glu-53(Q), the activation barrier is higher than 150 kJ mol^{-1}. These results apply to the proton transport from the active site to the protein surface. If the reverse direction is considered, the differences are not so high and the second pathway might be slightly preferred. Nevertheless, it is worth pointing out that the proton transport need not be limited (and probably is not) to a single pathway.

It is interesting to note that the results we obtain for the first pathway are in agreement with the results of a recent study by Teixeira *et al.*[21] They used Poisson–Boltzmann and Monte Carlo techniques to determine the pK_a values of protonatable groups within the protein combined with a distance-based network analysis to find likely pathways for the proton transport. Our two approaches are different, but complementary. That of Teixeira *et al.* defines pathways in terms of the ability of neighboring groups within the protein to accept or donate protons, whereas ours gives the detailed movements and energetics of the proton-transfer process within a predefined pathway. It would be of interest to apply our method to the other pathways mentioned by Teixeira *et al.* that we have not studied in this work.

The results obtained in this article and that of Teixeira *et al.* [21] are suggestive, but not decisive. First of all, only a limited set of possible pathways was examined, albeit the ones that were most evident by analysis of the crystallographic structures of the various [NiFe] hydrogenases, and it would be desirable to investigate other alternatives. Second, only "static" pathways have been considered, but the possibility exists that alternatives form by medium- or large-scale movements of the protein as is well known to occur in other cases involving molecular transport in proteins. Third, the methodology we have employed, while relatively sophisticated, could be improved by increasing the precision of the QM method and by including effects, such as QM tunneling, that have been neglected. All of this leaves the field open for further research.

REFERENCES

1. Vignais PM, Billoud B. Occurrence, classification, and biological function of hydrogenases: an overview. Chem Rev 2007;107:4206–4272.
2. Fontecilla-Camps JC, Volbeda A, Cavazza C, Nicolet Y. Structure/function relationships of [NiFe]- and [FeFe]-hydrogenases. Chem Rev 2007;107:4273–4303.
3. Montet Y, Amara P, Volbeda A, Vernede X, Hatchikian EC, Field MJ, Frey M, Fontecilla-Camps JC. Gas access to the active site of Ni-Fe hydrogenases probed by X-ray crystallography and molecular dynamics. Nat Struct Biol 1997;4:523–526.
4. Nicolet Y, Piras C, Legrand P, Hatchikian CE, Fontecilla-Camps JC. *Desulfovibrio desulfuricans* iron hydrogenase: the structure shows

unusual coordination to an active site Fe binuclear center. Structure 1999;7:13–23.
5. Cohen J, Kim K, Posewitz M, Ghirardi M, Schulten K, Seibert M, King P. Molecular dynamics and experimental investigation of H_2 and O_2 diffusion in [Fe]-hydrogenase. Biochem Soc Trans 2005;33:80–82.
6. Teixeira VH, Baptista AM, Soares CM. Pathways of H_2 toward the active site of [NiFe]-hydrogenase. Biophys J 2006;91:2035–2045.
7. Cammack R, Patil DS, Hatchikian EC, Fernández VM. Nickel and iron-sulphur centres in *Desulfovibrio gigas* hydrogenase: ESR spectra, redox properties and interactions. Biochim Biophys Acta 1987;912:98–109.
8. Albracht SPJ. Nickel hydrogenases: in search of the active site. Biochim Biophys Acta 1994;1188:167–204.
9. de Lacey AL, Hatchikian EC, Volbeda A, Frey M, Fontecilla-Camps JC, Fernández VM. Infrared-spectroelectrochemical characterization of the [NiFe] hydrogenase of *Desulfovibrio gigas*. J Am Chem Soc 1997;119:7181–7189.
10. Niu S, Thomson LM, Hall MB. Theoretical characterization of the reaction intermediates in a model of the nickel-iron hydrogenase of *Desulfovibrio gigas*. J Am Chem Soc 1999;121:4000–4018.
11. Amara P, Volbeda A, Fontecilla-Camps JC, Field MJ. A hybrid density functional theory/molecular mechanics study of nickel-iron hydrogenase: investigation of the active site redox states. J Am Chem Soc 1999;121:4468–4477.
12. Siegbahn PEM, Blomberg MR, Wirstam née Pavlov M, Crabtree RH. The mechanism of the Ni-Fe hydrogenases: a quantum chemical perspective. J Biol Inorg Chem 2001;6:460–466.
13. Volbeda A, Martin L, Cavazza C, Matho M, Faber BW, Roseboom W, Albracht SPJ, Garcin E, Rousset M, Fontecilla-Camps JC. Structural differences between the ready and unready oxidized states of [NiFe] hydrogenases. J Biol Inorg Chem 2005; 10:239–249. Erratum in J Biol Inorg Chem 2005;10:591.
14. Pardo A, De Lacey AL, Fernández VM, Fan HJ, Fan Y, Hall MB. Density functional study of the catalytic cycle of nickel-iron [NiFe] hydrogenases and the in-volvement of high-spin nickel(II). J Biol Inorg Chem 2006;11:286–306.
15. Williams RJP. Purpose of proton pathways. Nature 1995;376:643.
16. Brzezinski P, Ädelroth P. Design principles of proton-pumping haemcopper oxidases. Curr Opin Struct Biol 2006;16:465–472.
17. Volbeda A, Charon MH, Piras C, Hatchikian EC, Frey M, Fontecilla-Camps JC. Crystal structure of the nickel-iron hydrogenase from *Desulfovibrio gigas*. Nature 1995;373:580–587.
18. Matias PM, Soares CM, Saraiva LM, Coelho R, Morais J, Le Gall J, Carrondo MA. [NiFe] hydrogenase from *Desulfovibrio desulfuricans* ATCC 27774: gene sequencing, three-dimensional structure determination and refinement at 1.8 Å and modelling studies of its interaction with the tetrahaem cytochrome c_3. J Biol Inorg Chem 2001;6:63–81.
19. Volbeda A, Fontecilla-Camps JC. Structure-function relationships of nickel-iron sites in hydrogenase and a comparison with the active sites of other nickel-iron enzymes. Coord Chem Rev 2005;249:1609–1619.
20. Dementin S, Burla B, De Lacey AL, Pardo A, Adryanczyk-Perrier G, Guigliarelli B, Fernández VM, Rousset M. A glutamate is the essential proton transfer gate during the catalytic cycle of the [NiFe] hydrogenase. J Biol Chem 2004;279:10508–10513.
21. Teixeira VH, Soares CM, Baptista AM. Proton pathways in a [NiFe]-hydrogenase: a theoretical study. Proteins: Struct Funct Bioinf 2008;70:1010–1022.
22. Frey M, Fontecilla-Camps JC, Volbeda A. Nickel-iron hydrogenases. In: Messerschmidt A, Huber R, Wieghardt K, Poulos T, editors. Handbook of metalloproteins. Chichester: John Wiley & Sons, Ltd.; 2001. vol. 2, pp 880–896.
23. Humphrey W, Dalke A, Schulten K. VMD: Visual molecular dynamics. J Mol Graph 1996;14:33–38.
24. Higuchi Y, Ogata H, Miki K, Yasuoka N, Yagi T. Removal of the bridging ligand atom at the Ni—Fe active site of [NiFe] hydrogenase upon reduction with H_2, as revealed by X-ray structure analysis at 1.4 Å resolution. Structure 1999;7:549–556.
25. Garcin E, Vernede X, Hatchikian EC, Volbeda A, Frey M, Fontecilla-Camps JC. The crystal structure of a reduced [NiFeSe] hydrogenase provides an image of the activated catalytic center. Structure 1999;7:557–566.
26. Lubitz W, Reijerse E, van Gastel M. [NiFe] and [FeFe] hydrogenases studied by advanced magnetic resonance techniques. Chem Rev 2007;107:4331–4365.
27. Breneman CM, Wiberg KB. Determining atom-centered monopoles from molecular electrostatic potentials. The need for high sampling density in formamide conformational analysis. J Comput Chem 1990;11:361–373.
28. Wang H, Ralston CY, Patil DS, Jones RM, Gu W, Verhagen M, Adams M, Ge P, Riordan C, Marganian CA, Mascharak P, Kovacs J, Miller CG, Collins TJ, Brooker S, Croucher PD, Wang K, Stiefel EI, Cramer SP. Nickel L-edge soft X-ray spectroscopy of nickel-iron hydrogenases and model compounds—evidence for high-spin nickel(II) in the active enzyme. J Am Chem Soc 2001;122:10544–10552.
29. Fan HJ, Hall MB. High-spin Ni(II), a surprisingly good structural model for [NiFe] hydrogenase. J Am Chem Soc 2002;124:394–395.
30. Jorgensen WL, Maxwell DS, Tirado-Rives J. Development and testing of the OPLS all-atom force field on conformational energetics and properties of organic liquids. J Am Chem Soc 1996;118:11225–11236.
31. Li H, Robertson AD, Jensen JH. Very fast empirical prediction and rationalization of protein pK_a values. Proteins: Struct Funct Bioinf 2005;61:704–721.
32. Davis ME, Madura JD, Luty BA, McCammon JA. Electrostatics and diffusion of molecules in solution: simulations with the University of Houston Brownian dynamics program. Comput Phys Commun 1991;62:187–197.
33. Repasky MP, Chandrasekhar J, Jorgensen WL. PDDG/PM3 and PDDG/MNDO: Improved semiempirical methods. J Comput Chem 2002;23:1601–1622.
34. Jónsson H, Mills G, Jacobsen KW. Nudged elastic band method for finding minimum energy paths of transitions. In: Berne BJ, Cicotti G, Coker DF, editors. Classical and quantum dynamics in condensed phase simulatinns. Singapore: World Scientific 1998. chapter 16, pp 385–404.
35. Fdez. Galván I, Field MJ. Improving the efficiency of the NEB reaction path finding algorithm. J Comput Chem 2008;29:139–145.
36. Field MJ, Albe M, Bret C, Proust-De Martin F, Thomas A. The dynamo library for molecular simulations using hybrid quantum mechanical and molecular mechanical potentials. J Comput Chem 2000;21:1088–1100.
37. Frisch MJ, Trucks GW, Schlegel HB, Scuseria GE, Robb MA, Cheeseman JR, Zakrzewski VG, Montgomery JA Jr, Stratmann RE, Burant JC, Dapprich S, Millam JM, Daniels AD, Kudin KN, Strain MC, Farkas Ö, Tomasi J, Barone V, Cossi M, Cammi R, Mennucci B, Pomelli C, Adamo C, Clifford S, Ochterski JW, Petersson GA, Ayala PY, Cui Q, Morokuma K, Malick DK, Rabuck AD, Raghavachari K, Foresman JB, Cioslowski J, Ortiz JV, Baboul AG, Stefanov BB, Liu G, Liashenko A, Piskorz P, Komaromi I, Gomperts R, Martin RL, Fox DJ, Keith TA, Al-Laham MA, Peng CY, Nanayakkara A, Challacombe M, Gill PMW, Johnson B, Chen W, Wong MW, Andrés JL, González C, Head-Gordon M, Replogle ES, Pople JA. Gaussian 98 (Revision A.7). Pittsburgh, PA: Gaussian Inc., 1998.
38. Henkelman G, Jónsson H. Improved tangent estimate in the nudged elastic band method for finding minimum energy paths and saddle points. J Chem Phys 2000;113:9978–9985.
39. George SJ, Kurkin S, Thorneley RNF, Albracht SPJ. Reactions of H_2, CO, and O_2 with active [NiFe]-hydrogenase from *Allochromatium vinosum*. A stopped-flow infrared study. Biochemistry 2004;43:6808–6819.
40. Katz AK, Glusker JP, Markham GD, Bock CW. Deprotonation of water in the presence of carboxylate and magnesium ions. J Phys Chem B 1998;102:6342–6350.